Available online at www.sciencedirect.com
ScienceDirect
Journal of Sound and Vibration 320 (2009) 184–200
JOURNAL OF SOUND AND VIBRATION
www.elsevier.com/locate/jsvi

Experimental and theoretical simulations on wind–rain-induced vibration of 3-D rigid stay cables

M. Gu*, X.Q. Du, S.Y. Li

State Key Laboratory for Disaster Reduction in Civil Engineering, Tongji University, Shanghai, China

Received 20 September 2007; received in revised form 5 July 2008; accepted 12 July 2008
Handling Editor: L.G. Tham
Available online 27 August 2008

Abstract

In this paper, a cable model with an artificial rivulet model is tested with the help of a specially designed test set-up. Mean and fluctuating pressures and aerodynamic forces acting on the cable model and the artificial rivulet model under typical conditions are obtained and the formulas of the aerodynamic forces are derived. On the basis of the wind forces, a new theoretical model for describing wind–rain-induced vibration is established. In the theoretical model, equations governing the motions of the cable and rivulet models are both established, and a new description of friction force between the water rivulet and the cable surface is adopted. Then wind–rain-induced responses of a typical three-dimensional (3-D) rigid cable model are computed by using the present theoretical model. Some main computed results are compared with experimental ones of an elastically supported rigid cable model reported in literature. Finally, a possible mechanism of wind–rain-induced vibration of cables is suggested.

1. Introduction

There have been many reports in the past 20 years on excessive and unanticipated vibration of cables in cable-stayed bridges under the simultaneous occurrence of wind and rain [1–9]. The authors also observed wind–rain-induced cable vibration from cable-stayed bridges, which have been built in Shanghai [8] and Nanjing [9]. The bridges have main span of 602 and 628 m, respectively. Wind–rain-induced cable vibration has become a great concern to bridge engineering and wind engineering communities.

To investigate the characteristics and the mechanism of the complex phenomenon, field measurements [1,2,4,6,7,9], wind tunnel simulation tests [10–16] and theoretical analyses [17–24] were conducted by researchers. In wind tunnel simulation tests, there are mainly two approaches for simulating rivulet on cable section model: one is to spray water appropriately onto the surface of the cable model to form rivulet [10,15], and the other is to stick artificial rivulet model on the cable model surface [14,16–18]. Cosentino et al. measured wind pressures acting on a cable model under simulated wind and rain conditions and suggested a new concept of critical Re range for description of rain–wind-induced vibration of stay cables [16,23].

*Corresponding author. Tel./fax: +86 21 65981210.
E-mail address: minggu@mail.tongji.edu.cn (M. Gu).

0022-460X/$ - see front matter © 2008 Elsevier Ltd. All rights reserved.
doi:10.1016/j.jsv.2008.07.009

In theoretical studies, quasi-steady assumption was adopted by most of the researchers [17–23]. As another consideration, Matsumoto et al. [25] suggested an unsteady aerodynamic forces, which were expressed by aerodynamic derivatives, H_i^* ($i = 1$–4), to study the aerodynamic damping and the instability of cables. Moreover, Masumoto et al. [26] discovered that stay cables might vibrate at highly reduced wind speeds, such as 20, 40, 60 and 80, under wind–rain condition or only wind condition from field measurements, and raised an explanation of axial flow and axial vortexes as another possible mechanism of wind–rain-induced vibration. Through the studies, it has been suggested that the movement of upper rivulet on the cable surface could be the possible mechanism of the complex phenomenon. Even so, the mechanism of wind–rain-induced vibration has not been fully recognized so far.

This paper tries to develop a new theoretical model based on the quasi-steady assumption to investigate the mechanism of wind–rain-induced vibration. A wind tunnel test is first carried on a cable model with an artificial rivulet model to measure the aerodynamic forces acting on the cable and rivulet models. Equations governing the motions of the cable and the rivulet are then both established, based on which the vibration characteristics of the cable and the rivulet are investigated and a possible mechanism is suggested.

2. Wind tunnel test

2.1. Cable model and test condition

The stay cables in cable-stayed bridges usually have diameters from 10 to 18 cm. Moreover, from the field observations [8] and wind tunnel tests [15], it was found that the width of water rivulet was about 1–2 cm. This means that if the cable model and the artificial rivulet model for the wind pressure test in a wind tunnel had the same sizes with the actual ones, the small artificial rivulet model would make the measurement of wind pressures acting on the rivulet very difficult, even impossible. Therefore, the sizes of cable model and accordingly the artificial rivulet model for the wind tunnel test were both amplified for the test, about double or triple the actual ones. On the other hand, in order to assure the Re number of the model was the same with the actual cable, the test wind speed should be 1/2–1/3 of the wind speed at which the wind–rain-induced vibration of real stay cables usually appears. The diameter of the cable was thus determined to be 350 mm and the model length was 3.5 m. The testing wind speed ranged from 3 to 10 m/s; the Re number was thus accordingly from 7.04×10^4 to 2.35×10^5, which is similar to the actual one. In addition, the previous studies [14] indicated that the lower rivulet located generally behind the lower flow separation point and thus has little effect on the wind–rain-induced vibration of cables. Therefore, only the upper rivulet but not the upper and lower rivulets were taken into account in the design of the testing model. Furthermore, the effects of shape and size of water rivulet on the wind forces acting on cable models have experimentally investigated. The wind tunnel tests on three kinds of section shapes of water rivulet, including circle [17], rectangle [10] and arc [27], indicated the same trend of the aerodynamic forces for the different water rivulets. The authors measured wind forces acting on a cable model with artificial water rivulet of different sizes using high-frequency force balance technique in a wind tunnel and the results showed that differences of sizes of rivulets have almost no effects on the characteristics of rain–wind-induced vibration of the cables [14,18,20]. Also in the present paper, two kinds of artificial upper rivulets, which are schematically shown in Fig. 1, were adopted. In total, 176 pressure taps were arranged on the model in four sections (see Fig. 2a). The four sections were somewhat below the central

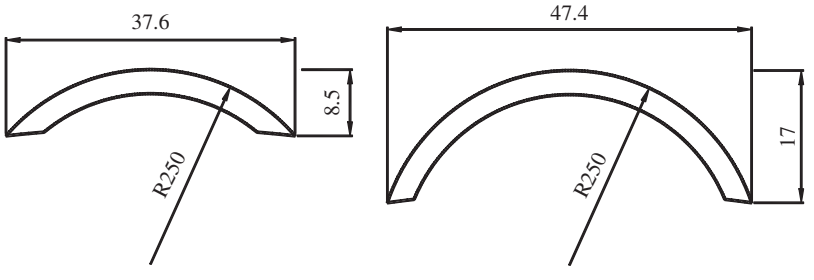

Fig. 1. Sizes of artificial rivulets (unit: mm).

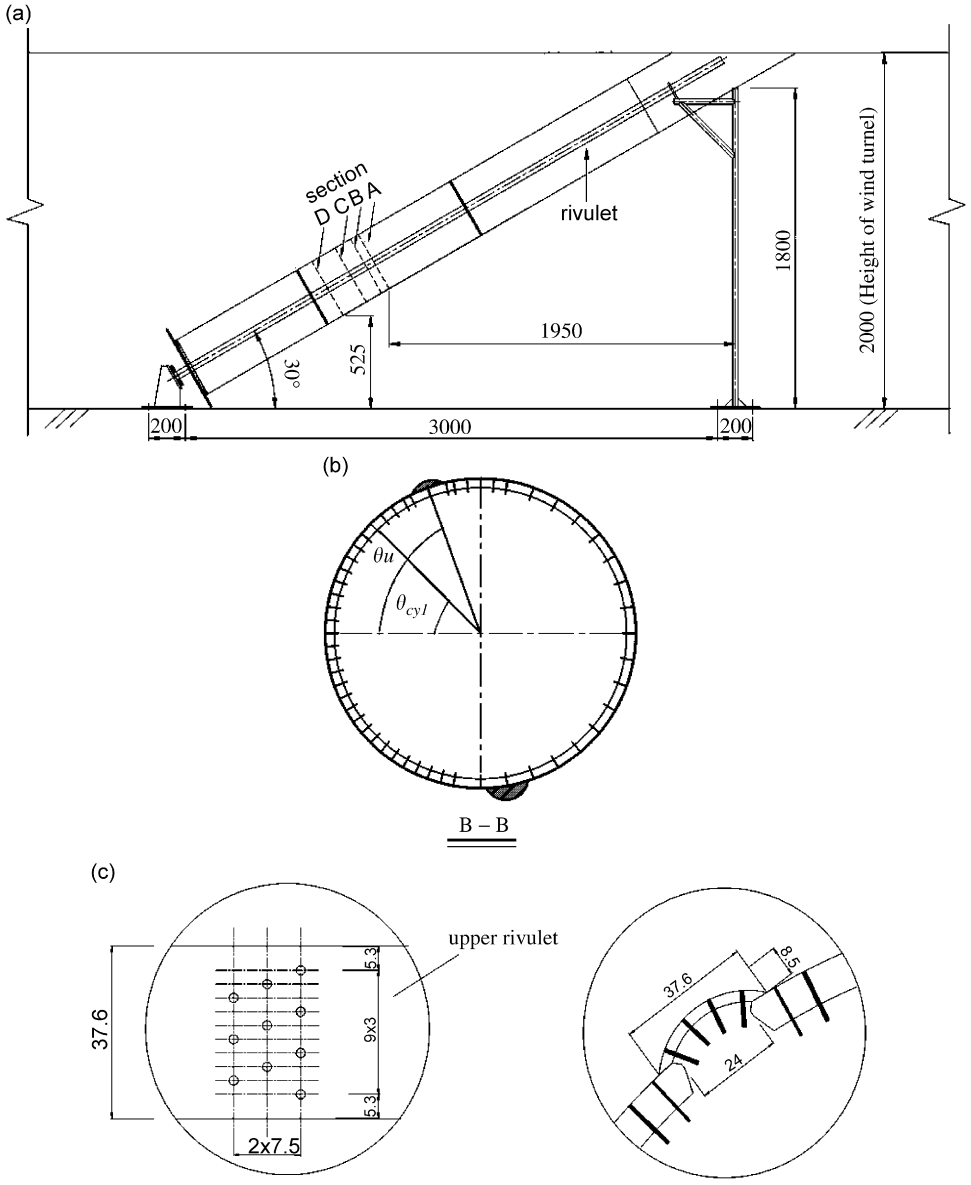

Fig. 2. Pressure tap arrangements: (a) Elevation of the model and four sections for pressure taps, (b) arrangement of pressure taps on section B and (c) arrangement of pressure taps on upper rivulet.

section of the whole model but the lowest pressure tap was 0.525 m above the wind tunnel floor to ensure the steady flow on these sections considering the definition of positive wind angle β, as is shown in Fig. 3. Fig. 3 also illustrates the inclined cable angle α. Furthermore, 63 pressure taps arranged on section B (sections A–D were denoted from top to bottom in Fig. 2a) are shown in Fig. 2b. Especially, to understand detailed information of wind pressures on the rivulet, the pressure taps were arranged in three rows on the rivulet model (see Fig. 2c).

The test was carried out in smooth flow in TJ-3 BLWT in Tongji University, which has a working section of 15 m in width and 2 m in height. The experimental set-up was specially designed for the test, which was mounted on the rotating table of the wind tunnel. The cable model can be easily adjusted to the required wind

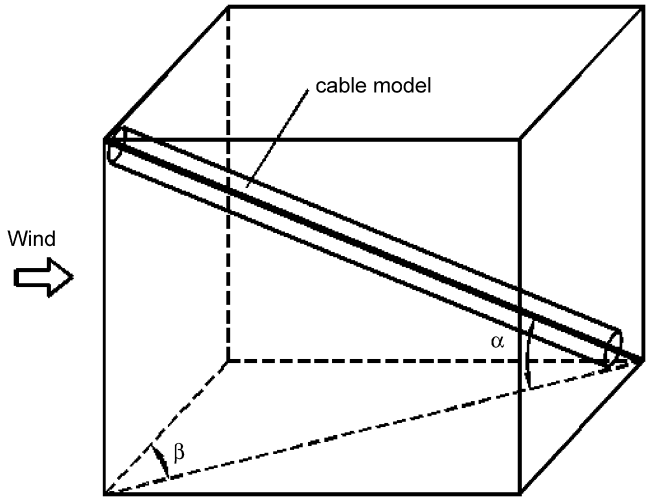

Fig. 3. 3-D rigid cable model described by inclined cable angle α and wind angle β.

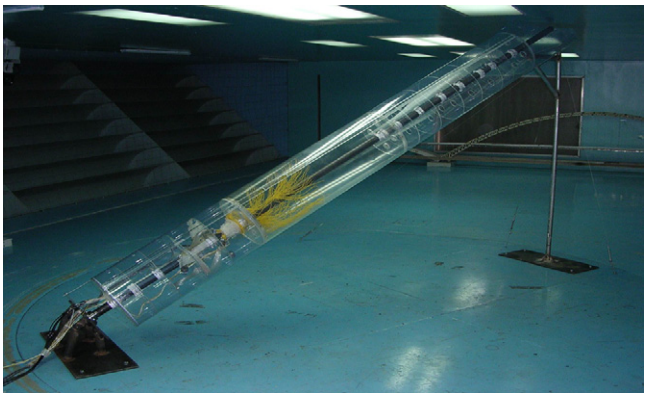

Fig. 4. Photo of test set-up and model.

angles and cable's inclined angles. The cable model was smoothly extended to the top of wind tunnel to avoid the flow separation at the top of the cable model to simulate the flow behavior of a very long cable. Fig. 4 shows the photograph of the test set-up and the model. According to the previous wind tunnel test results [15], stay cables may be prone to wind–rain-induced vibration commonly under the condition of inclined cable angle of about 30° and the wind directions ranging from 20° to 40°. So, the cable inclined angle was fixed at 30° and the wind directions were 0°, 25°, 30°, 35°, 40° and 45° in the test. Furthermore, in order to measure the wind pressures under the condition of the rivulet being at different locations, which is denoted by θ_u (see Fig. 2c), the cable model can rotate around its axis to make the rivulet model at different positions. The previous wind tunnel tests [17,18] indicated that the aerodynamic forces could increase or decrease violently when the upper rivulet varied even slightly around its critical position. Therefore, in the present test, the increment interval of the upper rivulet was 2° for the upper rivulet ranging from 30° to 82°, while 4° for the upper rivulet in the other range.

A DSM3000 electronic pressure scan valve system was used to measure the wind pressures acting on the cable and rivulet models. The sampling frequency was 312.5 Hz, and the measuring duration was 30 s. A transfer function method [28] was adopted to correct the distortion of fluctuating wind pressures passing

through the measuring tubes. The test results show that the mean and fluctuating wind pressures on the four sections are almost the same, so only the pressures on section B are applied herein.

2.2. Main test results

As is expected, the wind pressures acting on the cable for the two kinds of different artificial rivulets have the similar trends, which have also been pointed out in Refs. [14,18]. Therefore, only the main results of wind pressures and wind forces acting on the cable model with the smaller artificial rivulet, are presented. Moreover, because the pressure data from the test are too many to be totally presented here, only the results for the case of 30° cable inclined angle and 35° wind direction angle are shown, herein as the basis of the following theoretical model and the computation of the cable response. More detailed testing results can be found in Ref. [29].

2.2.1. Typical wind pressures on cable and rivulet model

Fig. 5 illustrates the mean and fluctuating wind pressure coefficients of the cable model and the rivulet model for typical upper rivulet positions. The position of the pressure point is denoted by θ_{cyl}. When the upper rivulet is located at 0°, i.e., $\theta_u = 0°$, the standing point goes down to 340° (i.e., −20°) for the present three-dimensional (3-D) cable model; and accordingly the mean wind pressure coefficient at the standing point is somewhat smaller than that of a two-dimensional (2-D) circular cylinder [29]. When the upper rivulet ranges from 10° to 46°, the absolute values of the mean wind pressures at the tap positions just behind the upper rivulet suddenly become much larger than those in the front of the upper rivulet; while those at the other tap positions are almost unvaried. When the upper rivulet position is located in the range of 48–90°, which means the rivulet is behind the separation point, the effects of the rivulet on the wind pressure distribution become less significant. From Fig. 5, it can also be seen that the rms fluctuating wind pressure coefficients at most of the pressure taps are small and can hardly affected by the rivulet. Fig. 6 shows power spectrum density of fluctuating wind pressures at one typical position ($\theta_{cyl} = 246°$). From the figure of power spectrum density of fluctuating wind pressure at the selected point, one can see that besides a peak at the non-dimensional frequency of 0.17–0.2, which may be caused by Karmen vortexes shed from the cable model, and several other peaks appear with lower frequencies, which may be explained as the axis flow and axial vortex [26]. From the discussions above, the upper rivulet has great effects on the mean wind pressure distributions of the cable model.

2.2.2. Aerodynamic forces on cable and rivulet models

The coordinate system of the model and the directions of the aerodynamic forces are schematically illustrated in Fig. 7. The x coordinate is parallel to the ground and perpendicular to the axial plan of the cable model; and the y coordinate is also perpendicular to the model's axis. The axial plan of the cable model is along the model's axis and perpendicular to the ground. The initial angle and instantaneous position angle of the rivulet are denoted by θ_0 and θ, respectively. The aerodynamic forces can be obtained through integrating the wind pressures over all the taps. The variations of the mean lift and drag coefficients, C_L and C_D, of the cable model with different upper rivulet positions for the typical wind direction angles are presented in Fig. 8. For the upper rivulet positions smaller than 44°, the lift and drag coefficients are from 0.4 to 0.6; and for the rivulet position ranging between 44° and 48°, the drag and lift coefficients suddenly increases and decreases, respectively, especially for the cases of wind directions angles of 25° and 35°. This might indicate that the zone of $\theta_u (= \theta + \theta_0)$ from 44° to 48° may be the aerodynamic unstable zone. In fact, the authors found in Ref. [15] that vibration amplitudes for the cases of 25° and 35° wind directions are obviously larger than those for the other wind directions. For convenience of the later application of theoretical model, formulas of the mean lift and drag coefficients are fitted as a function of $\phi' = \phi + \theta + \theta_0$ (see Fig. 7) using least-squares technique. The formulas cover a much wider range than the range from 44° to 48° of the upper rivulet position. Only the formulas of lift and drag coefficients for the condition of cable inclined angle of 30° and wind angle of 35° (γ is defined in Fig. 7. For the conditions of $\alpha = 30°$ and $\beta = 35°$, $\gamma = 19.3°$) are presented as follows:

For $0.337 \leqslant \phi' \leqslant 1.174$ (radian),

$$C_D(\phi') = 414.612 - 5874.960\phi' + 36063.162\phi'^2 - 125707.500\phi'^3 + 274498.563\phi'^4 - 389948.057\phi'^5 + 360930.20381\phi'^6 - 210205.891\phi'^7 + 69997.4332\phi'^8 - 10166.924\phi'^9 \quad (1a)$$

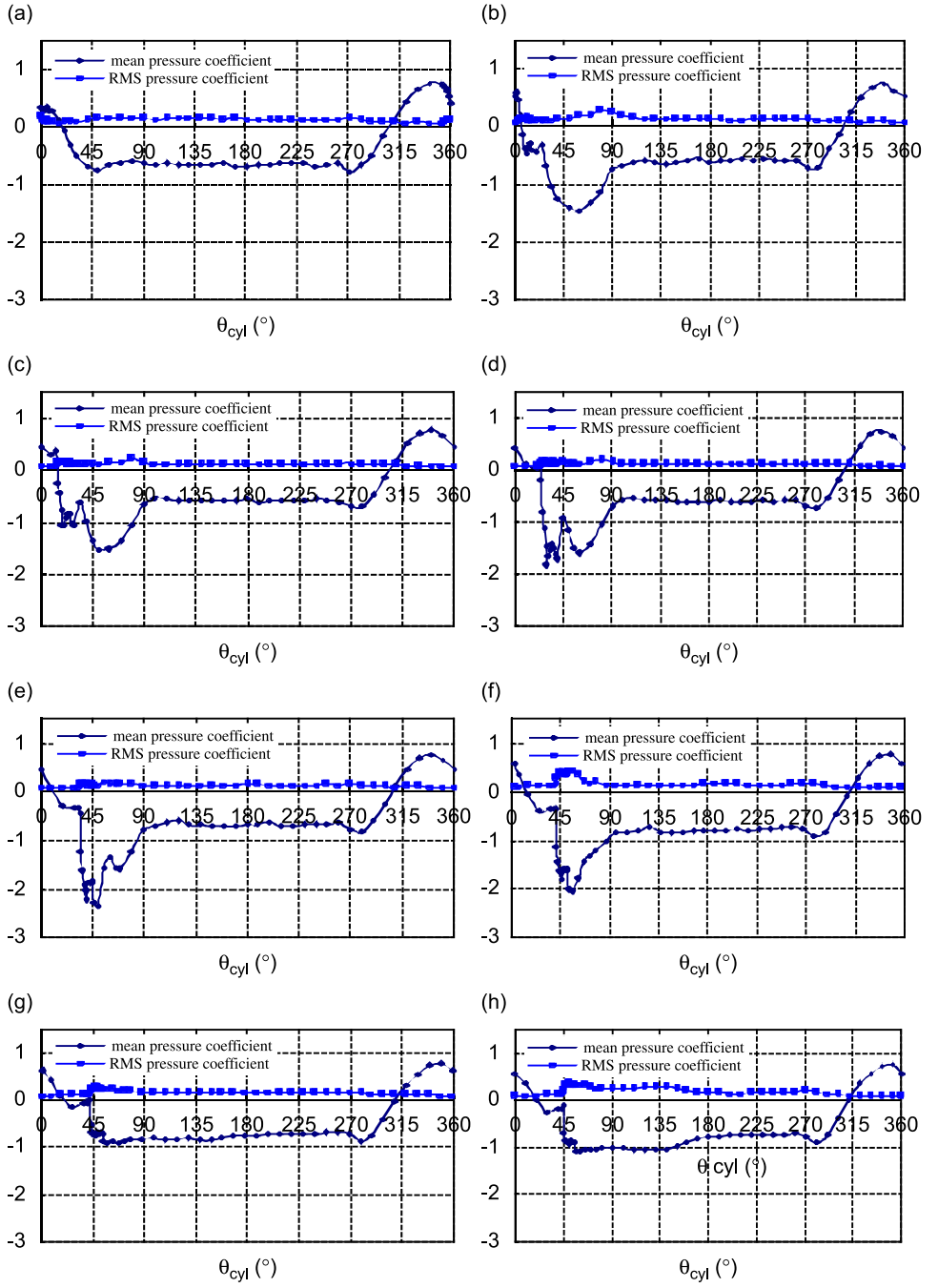

Fig. 5. Wind pressure coefficients on cable model and rivulet model ($\beta = 350$, Re = 1.2e5): (a) $\theta_u = 0°$, (b) $\theta_u = 10°$, (c) $\theta_u = 20°$, (d) $\theta_u = 30°$, (e) $\theta_u = 40°$, (f) $\theta_u = 46°$, (g) $\theta_u = 48°$, (h) $\theta_u = 50°$, (i) $\theta_u = 60°$, (j) $\theta_u = 70°$, (k) $\theta_u = 80°$ and (l) $\theta_u = 90°$.

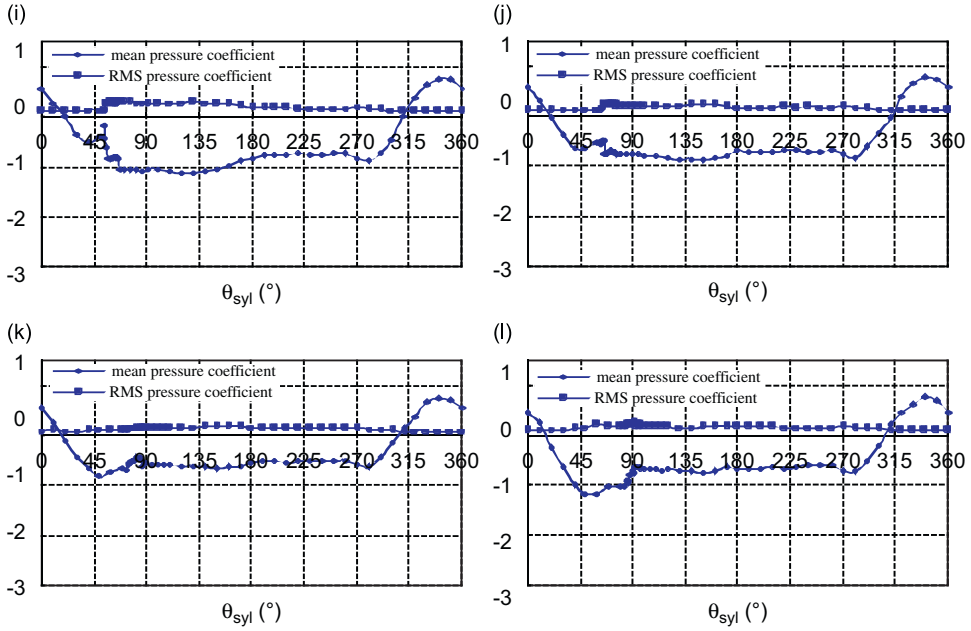

Fig. 5. (*Continued*)

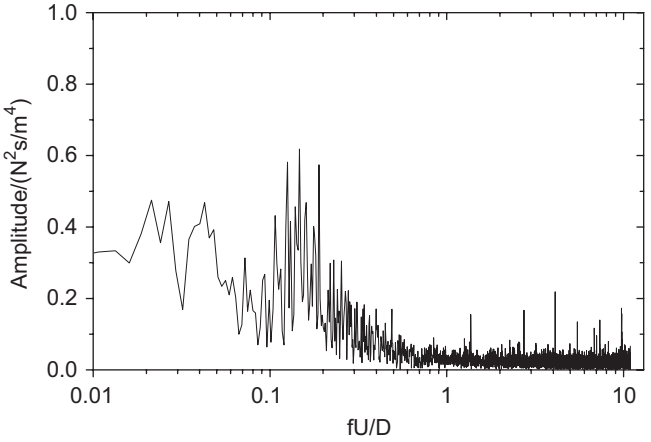

Fig. 6. PSD of wind pressures at typical point. $\theta_u = 46^\circ$, $\theta_{\mathrm{cyl}} = 246^\circ$.

$$C_L(\phi') = 89.308 - 1241.370\phi' + 7479.664\phi'^2 - 25870.496\phi'^3 + 56997.146\phi'^4 - 83166.040\phi'^5 + 80355.099\phi'^6 - 49500.190\phi'^7 + 17608.969\phi'^8 - 2751.762\phi'^9 \quad (1b)$$

and for $1.174 < \phi' \leqslant 1.907$ (radian),

$$C_D(\phi') = -59.281 + 146.406\phi' - 130.364\phi'^2 + 50.418\phi'^3 - 7.164\phi'^4 \quad (2a)$$

$$C_L(\phi') = -138.187 + 364.113\phi' - 355.520\phi'^2 + 152.456\phi'^3 - 24.222\phi'^4 \quad (2b)$$

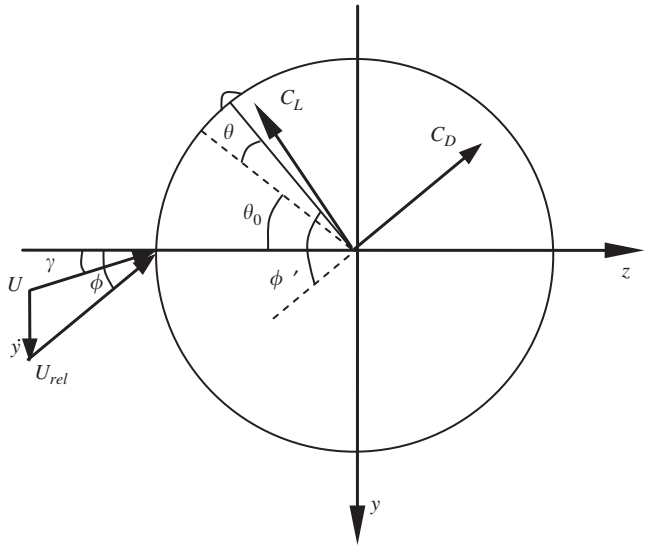

Fig. 7. Coordinate system of the model and directions of aerodynamic forces.

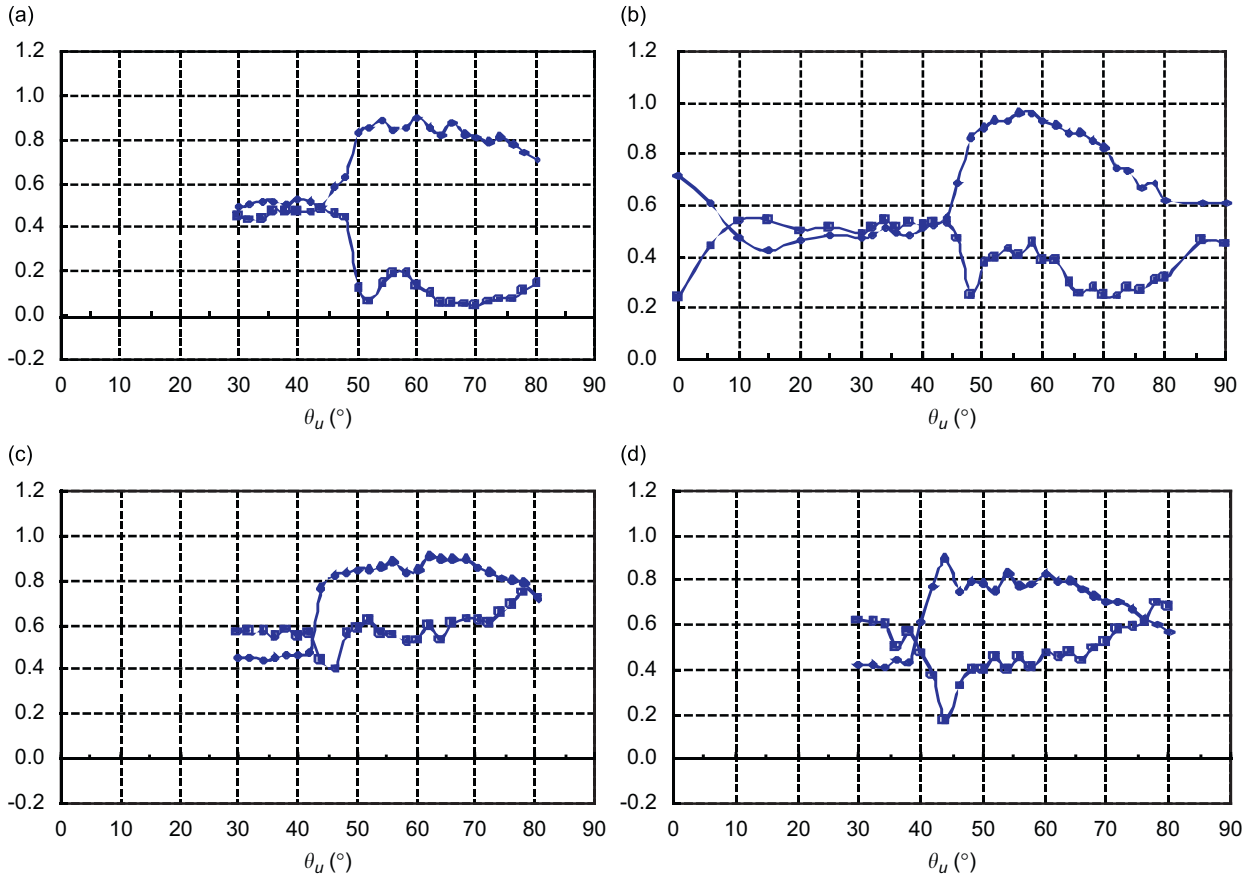

Fig. 8. Aerodynamic force coefficients of cable (-◆- C_D; -■- C_L). (a) $\beta = 25°$, (b) $\beta = 35°$, (c) $\beta = 40°$ and (d) $\beta = 45°$.

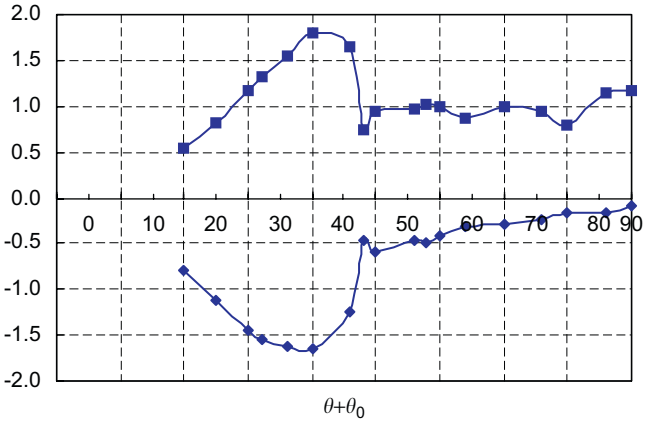

Fig. 9. Aerodynamic force coefficients of rivulet (-◆- c_l; -■- c_d).

Fig. 9 presents the mean lift and drag coefficients, c_l and c_d, of the rivulet for the condition of cable inclined angle of 30° and wind angle of 35°. The fitted formulas are as follows:

For $0.337 \leqslant \phi' \leqslant 1.174$ (radian),

$$c_d(\phi') = -556.828 + 3077.682\phi' - 6752.521\phi'^2 + 7350.843\phi'^3 - 3976.649\phi'^4 + 856.480\phi'^5 \tag{3a}$$

$$c_l(\phi') = -5080.425 + 34688.718\phi' - 98080.616\phi'^2 + 146999.950\phi'^3 - 123178.026\phi'^4 + 54728.168\phi'^5 - 10075.677\phi'^6 \tag{3b}$$

and for $1.174 < \phi' \leqslant 1.907$ (radian),

$$c_d(\phi') = 11668.679 - 54592.670\phi' + 109115.881\phi'^2 - 120775.568\phi'^3 + 79945.337\phi'^4 - 31642.867\phi'^5 + 6933.343\phi'^6 - 648.674\phi'^7 \tag{4a}$$

$$c_l(\phi') = -479.655 + 1562.689\phi' - 2030.702\phi'^2 + 1319.811\phi'^3 - 429.234\phi'^4 + 55.884\phi'^5 \tag{4b}$$

The above formulas of the aerodynamic forces will be used in the theoretical model of wind–rain-induced vibration of stay cables in the following text.

3. Theoretical formulation of wind–rain-induced vibration

3.1. Basic assumptions

As is well known, the wind–rain-induced vibration of stay cables in cable-stayed bridges is a complex phenomenon. In order to appropriately and rationally simplify the mathematical model of the wind–rain-induced vibration of stay cables, the basic assumptions are made according to previous field measurements and wind tunnel tests as follows:

(a) The cable vibrates with a single mode.
(b) The effects of axial flow and axial vortexes are not taken into account in the present analysis tentatively.
(c) The quasi-steady assumption is applied in the present analysis, which is similar to the classical galloping. For common stay cables, the lower modal resonant wind speed due to a Karmam vortex excitation may be generally lower than 2–3 m/s according to the Strouhal number and parameters of common cables. Obviously, the resonance wind speed due to the Karmam vortex excitation is generally much lower than

the onset wind speed of wind–rain-induced vibration. Furthermore, although researchers tried to explain the mechanism of wind–rain-induced vibration according to unsteady forces acting on cables [22], more researchers [16,17,20,21] adopted the quasi-steady assumption to the aerodynamic forces for wind–rain-induced vibration.

3.2. Motion equations of cable and rivulet

The space stage of the 3-D cable is described by the inclined angle α and the wind direction angle β, as is illustrated in Fig. 4. The oncoming wind speed is denoted by U_0, which is not perpendicular to the axis of the cable due to the inclined angle of cable and the wind direction angle. U_0 can be decomposed into two parts. One is perpendicular to the axis of cable; and the other is parallel to the axis, which has less effect on the wind–rain-induced vibration. The first part is

$$U = U_0\sqrt{\cos^2\beta + \sin^2\alpha\sin^2\beta} = U_0\sqrt{\sin^2\alpha + \cos^2\alpha\cos^2\beta} \tag{5}$$

Moreover, the included angle γ between U and the horizontal plan (see Fig. 7) can be found from the following equation:

$$\gamma = \arcsin\left(\frac{\sin\alpha\,\sin\beta}{\sqrt{\cos^2\beta + \sin^2\alpha\sin^2\beta}}\right) \tag{6}$$

For the present conditions of 30° cable inclined angle and 35° wind direction, γ equals to 19.3°.

If the motion velocity of the cable in y direction is denoted by $\dot{y}$, the relative velocity U_{rel} is

$$U_{\mathrm{rel}} = \sqrt{(U\cos\gamma)^2 + (\dot{y} + U\sin\gamma)^2} \tag{7}$$

Thus, the included angle ϕ between the relative wind speed U_{rel} and the horizontal plan is

$$\phi = \arctan\left(\frac{\dot{y} + U\sin\gamma}{U\cos\gamma}\right) \tag{8}$$

As is discussed in Ref. [18], the forces acting on the cable are: the elastic force of cable itself; the structural damping force; the inertial force of cable; the aerodynamic forces; the gravity force; the friction force (damping force) between the cable surface and rivulet. The friction force is much smaller than the other forces acting on the cable and thus is omitted in the following equation governing the motion of the cable model. On the other hand, when the water rivulet moves around the surface of the vibrating cable, the forces acting on the rivulet are the inertial forces caused by the cable's motion and the rivulet motion itself, the rivulet's gravity force, the aerodynamic forces and the friction force between the water rivulet and the cable's surface, which is the reaction of the friction force acting on the cable model mentioned above. The friction (damping) force is here defined in the form of $F_0 + c_r R\dot{\theta}$, where F_0 is the static damping force and $c_r R\dot{\theta}$ is the linear damping force, based on the analysis of infiltration characteristics of water and solid surface [30]. The analysis of infiltration characteristics between water and solid surface [30] indicates there must be an interaction force between the solid and the water drop even if there is no relative motion between the water drop and the solid surface and, furthermore, the force could be tentatively considered to be constant. This force has the same expression as Coulomb damping force which was originally used to describe the interaction force between two solid objects and thus is also hereafter referred to as Coulomb damping force. As for the value of the Coulomb damping force, it is presently difficult to determine precisely. In this paper, the Coulomb damping force is assumed to be 5–40% of the water rivulet gravity, which is a rather wide range. To make up for this disadvantage, the effect of the Coulomb damping force on the rain–wind-induced vibration of cables will be numerically discussed in the following text. Furthermore, the magnitude of linear damping coefficient c_r is also difficult to determine. Peil and Nahrath [31] have discussed the characteristics of c_r and suggested the value of $0.05\,\mathrm{N\,s/m^2}$ ($d_\varphi = c_r R = 0.5\,\mathrm{N\,s/m}$). Recently, Peil and Dreyer [27], Lemaitre et al. [32] studied it by virtue of Navier–Stokes equations. In the present paper, c_r is selected to be 0.0008, 0.1, $1.0\,\mathrm{N\,s/m^2}$, which cover the

value suggested by Peil and Nahrath [31]. In fact, a great quantity of computation by the authors indicate that the cable's vibration is not sensitive to the linear damping coefficient, and thus no results about the effects of linear damping coefficient on the cable vibration will be presented in this paper.

The friction force defined in the present paper is somewhat different from that in Ref. [5] and other literatures. In the cable's motion equation, this force can be neglected, as is mentioned above, but in the rivulet motion equation, this force plays an important role.

Based on the discussions above, the equation governing the cable motion in the y direction can thus be written as

$$\ddot{y} + 2\zeta_y \omega_y \dot{y} + \omega_y^2 y = -F_y/M \tag{9}$$

where y is the dynamic displacement of the cable, ζ_y and ω_y the damping ratio and circular frequency of the cable, respectively and F_y the wind force acting on the cable which may lead to the wind–rain-induced cable vibration. According to the characteristics of forces acting on the cable model discussed above, the aerodynamic force $F_y(t)$ can be written as

$$F_y(t) = \tfrac{1}{2}\rho D U^2 C_y = F_L(\phi')\cos(\phi) + F_D(\phi')\sin(\phi) \tag{10}$$

were ρ is the air density, D the cable's diameter, F_L and F_D the lift and drag forces acting on the cable, respectively:

$$F_L = \tfrac{1}{2}\rho D U_{\mathrm{rel}}^2 C_L(\phi'), \tag{11}$$

and

$$F_D = \tfrac{1}{2}\rho D U_{\mathrm{rel}}^2 F_D(\phi') \tag{12}$$

Therefore,

$$F_y(t) = \tfrac{1}{2}\rho D U_{\mathrm{rel}}^2 [C_L(\phi')\cos(\phi) + C_D(\phi')\sin(\phi)] \tag{13}$$

where C_L and C_D are the lift and drag coefficients of the cable, respectively, which are presented above, i.e., Eqs. (1) and (2).

According to the discussion above of the forces acting on the rivulet, the motion equation of the rivulet in tangential direction can be written as

$$mR\ddot{\theta} + F_0 + c_r R\dot{\theta} = f_\tau(z) + m\ddot{y}\cos\theta - mg\cos\alpha\cos\theta \tag{14}$$

where m and R are the mass per unit length and characteristic size of the rivulet, respectively, F_0 and c_r are the Coulomb damping force and linear damping coefficient between the cable surface and the rivulet, $f_\tau(z)$ is the aerodynamic force acting on the rivulet:

$$f_\tau(z) = \tfrac{1}{2}\rho U_{\mathrm{rel}}^2 R[c_d \sin(\phi') + c_l \cos(\phi')] \tag{15}$$

c_d and c_l are the drag and lift coefficients of the rivulet, respectively, the fitted formulas of which are Eqs. (3) and (4).

The wind–rain-induced vibration of stay cables can be computed through the equations from Eqs. (9) to (15).

4. Numerical example and mechanism discussion

The cable model used in Ref. [15] to experimentally investigate the wind–rain-induced vibration of cables is adopted here to theoretically study the characteristics of the complex phenomenon and the mechanism. The cable model in Ref. [15] has a length 2.5 m and a diameter of 120 mm. The model's weight is 15 kg; the damping ratio is 0.14%; and thus the Scruton number is 5.86. Moreover, the frequency of the model system is 1 Hz. The rivulet's parameters are assumed to be Coulomb damping force between 0.005 and 0.04 N/m, i.e., 5–40% of rivulet's gravity [30] and the linear damping coefficient of 0.0008 N s/m^2. Moreover, it is assumed that the rivulet can form on the cable's surface for the rivulet position in the range between 0° and 90°, and when the rivulet is out of the range the rivulet vanishes and the computation will stop.

4.1. Responses of cable and rivulet

The vibration characteristics of the cable and the rivulet at different wind velocities are first computed. The wind velocities for the computations are $U_0 = 7.0$, 7.2, 7.3, 7.4, 7.5, 7.6, 7.8, 8.0, 8.3, 8.5, 8.8, 9.0, 9.1, 10.0, 11.0 and 12.0 m/s.

Fig. 10 presents the variation of vibration amplitude of the cable with wind velocity, together with the experimental results from Ref. [15]. From the figure, it can be clearly seen that the cable exhibits velocity- and amplitude-restricted response characteristics, which has also been pointed out [14,15]. Moreover, the onset velocities and amplitudes from the present computation and the wind tunnel test are comparable. Especially when the Coulomb damping coefficient is taken as 0.04 N/m, the amplitudes are much closer to the testing results in Ref. [15]. On the other hand, it was pointed out in Ref. [15] that the vibration characteristics of a cable model under the actions of wind and rain are very sensitive to the test conditions, and even under the "same" testing conditions the cable's vibration characteristics can exhibit somewhat different. In view of this situation, the comparison results shown in Fig. 10 seem to be acceptable.

The detailed computations provide the time histories of vibration amplitudes of the cable and rivulet, which are shown in Fig. 11. The results indicate that when the wind velocity is low the upper water rivulet cannot form on the cable's surface and the cable thus cannot vibrate. When the wind velocity ranges between 7.3 and 9.0 m/s, the upper water rivulet can form on the surface of the cable, between the upper and lower limits of "dangerous zone" ("dangerous zone" will be explained in the following text), and accordingly the cable has large vibration amplitudes. Furthermore, when the wind velocity increases to 9.1 m/s, the mean balance position of rivulet suddenly increases to a position out of the "dangerous zone", leading to stop of the vibration of the cable. More detailed discussions on the results in the figure will be made in the following text.

The power spectrum densities of the vibration displacements of the cable and the rivulet at different wind velocities are also computed and presented in Fig. 12. As can be seen in Fig. 12, only a narrow and high peak corresponding to the natural frequency of the cable at each of the wind velocities; while there are several peaks in the spectra of the rivulet's responses. Among the peaks in the spectra of the rivulet's responses, the first high peak corresponds to the natural frequency of the cable. The results seem to suggest that only when the dominant vibration frequency of the rivulet is the same as that of the cable, the cable can vibrate; or in other words, if the dominant vibration frequency of the rivulet is far away from the frequency of the cable, the cable is stable.

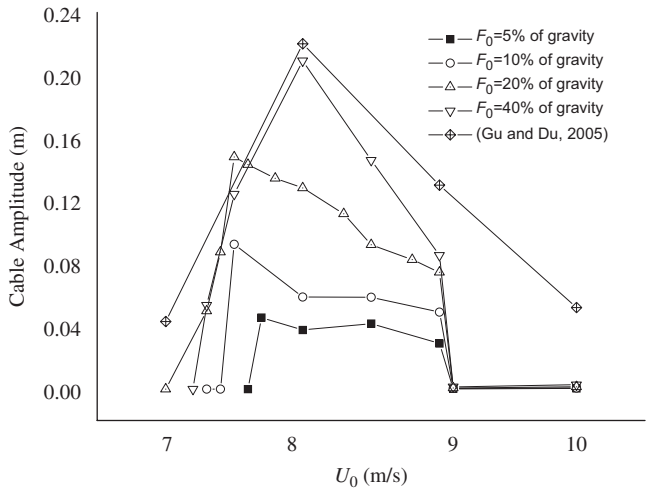

Fig. 10. Comparison between responses of cable from present computation and test [15].

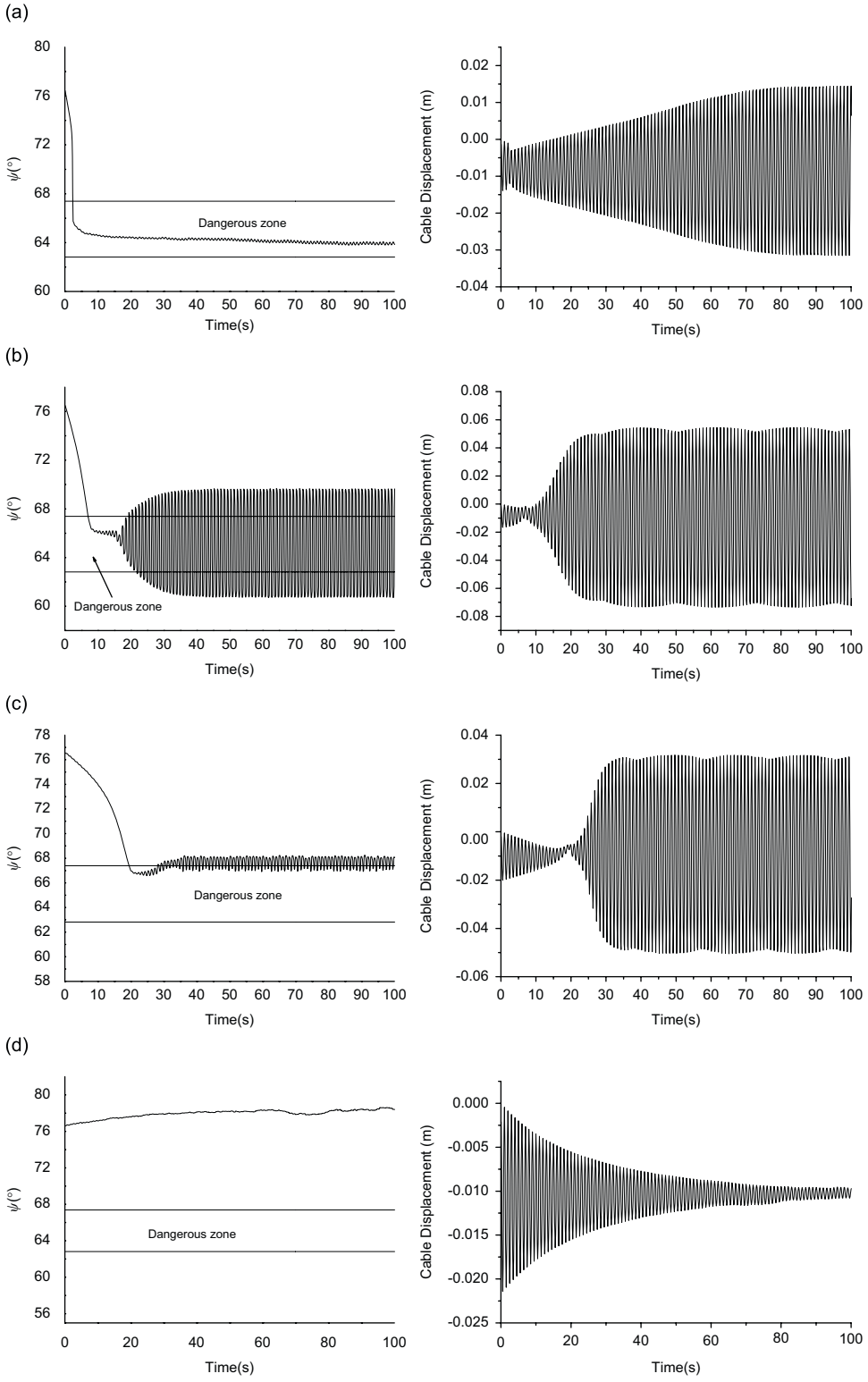

Fig. 11. Time histories of vibration displacements of cable and rivulet at typical wind velocities: (a) $U_0 = 7.3\,\mathrm{m/s}$, (b) $U_0 = 8.0\,\mathrm{m/s}$, (c) $U_0 = 8.8\,\mathrm{m/s}$ and (d) $U_0 = 9.1\,\mathrm{m/s}$.

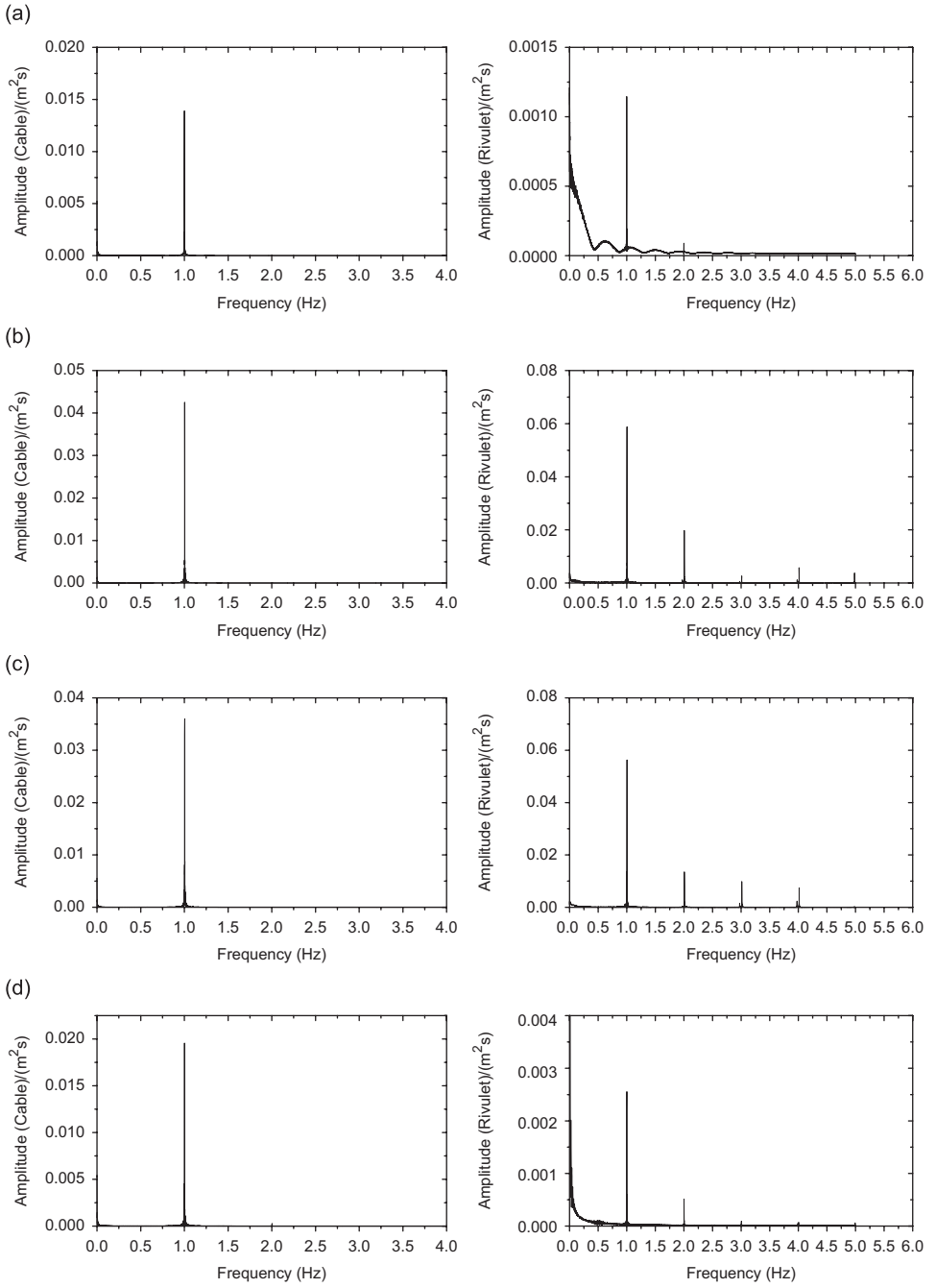

Fig. 12. Power spectrum densities of vibration responses of cable (left) and rivulet (right): (a) $U_0 = 7.3\,\text{m/s}$, (b) $U_0 = 7.6\,\text{m/s}$, (c) $U_0 = 7.8\,\text{m/s}$ and (d) $U_0 = 9.0\,\text{m/s}$.

4.2. Possible mechanism of wind–rain-induced vibration

The mechanism of wind–rain-induced vibration is discussed here according to Fig. 11. In order to make the discussion, some concepts are firstly introduced. The first two are the initial position and the instantaneous motion position of the rivulet, as is defined above. The former is the rivulet's position in computation time of zero; and the latter is the position of the vibrating rivulet at arbitrary time.

The study performed by the authors in Ref. [17] suggested an explanation of mechanism of wind–rain-induced vibration of a 2D cable. The suggested mechanism for of wind–rain-induced vibration of a 2-D cable seems still to be proper for the explanation of mechanism of a 3-D cable. From the present detailed computations, the authors find that there might exist an "unstable zone" of the initial rivulet position and a "dangerous zone" of the instantaneous rivulet position. The "unstable zone" means that when the rivulet is initially located at this zone, the aerodynamic forces acting on the rivulet might make the rivulet move to the "dangerous zone". And the "dangerous zone" is the negative slope zone of the galloping force coefficient, i.e., $C_D + \mathrm{d}C_L/\mathrm{d}\theta < 0$. When the rivulet's instantaneous position reaches the "dangerous zone", the vibrating cable can absorb energy from the aerodynamic force, which is similar to the phenomenon of galloping, and as a result, the vibration amplitudes of rivulet and cable will increase till very large amplitudes take place. For the present model, the "dangerous zone" of $\theta_u (= \theta + \theta_0)$ is from 44° to 48°. As is indicated above, for the conditions of cable inclination angle of 30° and wind yaw angle of 35°, $\gamma = 19.3$. Therefore, when a new angle ψ is defined to be the sum of γ, θ_0 and θ, that is, $\psi = \gamma + \theta_0 + \theta$, the "dangerous zone" of ψ ranges between 63° and 68°, which can be seen in Fig. 11. Obviously, the "unstable zone" is generally much wider than the corresponding "dangerous zone".

4.3. Discussion on damping force between cable and rivulet

Different from the theoretical models of wind–rain-induced vibration of cables in previous studies [18,20], the present model adopts a new damping force between the rivulet and the cable surface, which consists of the Coulomb damping force and linear damping force, as mentioned above. But unfortunately, it seems to be difficult to determine the value of the Coulomb damping force F_0. In order to investigate the effect of Coulomb damping force on the wind–rain-induced vibration of cables, four different values of the Coulomb damping force, which are 5%, 10%, 20% and 40% of the gravity of water rivulet per unit length, are adopted to compute the cable's response. Fig. 13 presents the relationship between the vibration peak amplitude of the rivulet and the Coulomb damping forces. The peak amplitude for the case of the Coulomb damping force of 0.02 N/m is largest, while that for the Coulomb damping force of 0.04 N/m seems to be smallest, which results in the vibration amplitude of the cable model matching the experimental one reported in Ref. [15] best, as is shown in Fig. 11. It seems to be difficult to appropriately explain the relationship between the vibration amplitudes of cable and rivulet.

Besides the Coulomb damping, the effects of linear damping coefficient on the vibration amplitude of cables are investigated as well. Three linear damping force coefficients adopted in the analysis are $c_r = 0.0008$, 0.1 and 1.0, and the Coulomb damping force takes 0.02 N/m. The computed results show that the vibration

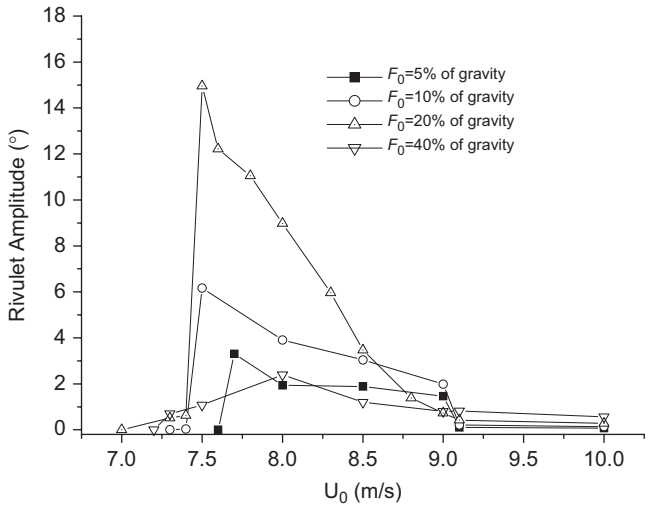

Fig. 13. Vibration amplitude vs. wind speed for the different Coulomb damping forces.

amplitude increases with the increase of linear damping force; but the effect of the linear damping on the cable amplitude is much less than the effect of the Coulomb damping force. For the linear damping force coefficient c_r increases from 0.0008 to 0.1, the cable vibration amplitude increases only 2 cm.

5. Concluding remarks

This paper studies wind–rain-induced vibration of cables of cable-stayed bridges based on quasi-steady assumption. Through the wind tunnel test on a 3-D sectional cable model, the wind pressures and mean wind forces acting on the cable model and upper artificial rivulet model are obtained. Violent variations of the wind forces acting on the cable model may be the key aerodynamic factors of wind–rain-induced vibration of cables. The wind forces are then used to develop a new theoretical model for wind–rain-induced vibration of 3-D cables. In the theoretical models, the equations governing motions of cable and rivulet are both derived and the damping force between the cable surface and the rivulet are considered to be composed of the Coulomb damping force and linear damping force. Some main computed results are compared with experimental ones of an elastically supported rigid cable model reported in literature. The comparison results are satisfied. The present theoretical model for wind–rain-induced vibration of 3-D cables seems to be able to estimate the vibration responses and the onset wind speed of cables. Finally, a possible mechanism of wind–rain-induced vibration of cables is suggested.

Acknowledgements

This project is financially supported by the China National Science Foundation (50621062) to which the writers gratefully appreciate.

References

[1] Y. Hikami, N. Shiraishi, Rain–wind induced vibrations of cables in cable stayed bridges, *Journal of Wind Engineering and Industrial Aerodynamics* 29 (1988) 409–418.
[2] K. Ohshima, M. Nanjo, Aerodynamics stability of the cables of a cable-stayed bridge subject to rain (a case study of the Aji River Bridge), *Proceedings of the US-Japan Joint Seminar on Natural Resources*, 1987, pp. 324–336.
[3] M. Matsumoto, T. Yagi, S. Sakai, J. Ohya, T. Okada, Aerodynamic force/aerodynamic response characteristics of inclined/yawed cable, *Proceedings of the 11th International Conference on Wind Engineering*, TX, USA, June 21–23, 2003.
[4] M. Matsumoto, Observed behavior of prototype cable vibration and its generation mechanism, in: A. Larsen, B. Esdahl (Eds.), *Bridge Aerodynamics*, Balkema, Rotterdam, 1998, pp. 189–211.
[5] B.M. Pacheco, Y. Fujino, Keeping cables calm, *Civil Engineering—ASCE* 63 (10) (1993) 56–58.
[6] J.A. Main, N.P. Jones, Full-scale measurements of stay cable vibration, in: A. Larsen, G.L. Larose, F.M. Liversey (Eds.), *Proceedings of the 10th International Conference on Wind Engineering*, Copenhagen, Denmark, 21–24 June 1999, pp. 963–970.
[7] A.J. Persoon, K. Noorlander, Full scale measurements on the Erasmus Bridge after rain/wind induced cable vibration, in: A. Larsen, G.L. Larose, F.M. Livesey (Eds.), *Proceedings of the 10th International Conference on Wind Engineering*, Copenhagen, Denmark, Vol. 2, 21–24 June 1999, pp. 1019–1026.
[8] M. Gu, C.J. Liu, G.Q. lou, Z.X. Lin, H.F. Xiang, Rain–wind induced vibration of cables on cable-stayed bridges and its control, *Shanghai Journal of Mechanics* 4 (1998) 281–288 (in Chinese).
[9] J.J. Shi, M. Gu, et al., Wind induced vibration of cables of Nanjing No. 2 Bridge over Yangtze River Research Report, Department of Bridge Engineering, Tongji University, 2003 (in Chinese).
[10] M. Matsumoto, T. Saitoh, M. Kitazawa, H. Shirato, T. Nishizaki, Response characteristics of rain–wind induced vibration of stay-cable of cable-stayed bridges, *Journal of Wind Engineering and Industrial Aerodynamics* 57 (1995) 323–333.
[11] M. Matsumoto, N. Shirashi, H. Shirato, Rain–wind induced vibration of cables of cable-stayed bridges, *Journal of Wind Engineering and Industrial Aerodynamics* 41–42 (1992) 2011–2022.
[12] O. Flamand, Rain–wind induced vibration of cables, *Journal of Wind Engineering and Industrial Aerodynamics* 57 (1995) 353–362.
[13] A. Bosdogianni, D. Olivari, Wind- and rain-induced oscillations of cables of stayed bridges, *Journal of Wind Engineering and Industrial Aerodynamics* 64 (1996) 171–185.
[14] M. Gu, C.J. Liu, Y.L. Xu, H.F. Xiang, Response characteristics of wind excited cable with artificial rivulet, *Applied Mathematics and Mechanics* 23 (10) (2002) 1176–1187.
[15] M. Gu, X.Q. Du, Experimental investigation of rain–wind-induced vibration of cables in cable-stayed bridges and its mitigation, *Journal of Wind Engineering and Industrial Aerodynamics* 93 (2005) 79–95.

[16] N. Cosentino, O. Flamand, C. Ceccoli, Rain–wind induced vibration of inclined stay cables—part 1: experimental investigation and physical explanation, *Wind and Structures* 6 (6) (2003) 471–484.
[17] H. Yamaguchi, Analytical study on growth mechanism of rain vibration of cables, *Journal of Wind Engineering and Industrial Aerodynamics* 33 (1990) 73–80.
[18] M. Gu, Q. Lu, Theoretical analysis of wind–rain induced vibration of cables of cable-stayed bridges, *Journal of Wind Engineering* 89 (2001) 125–128.
[19] K. Wilde, W. Witkowski, Simple model of rain–wind-induced vibrations of stayed cables, *Journal of Wind Engineering and Industrial Aerodynamics* 91 (2003) 873–891.
[20] M. Gu, L. Huang, Theoretical and experimental studies on aerodynamic instability of two-dimensional circular cylinder with moving attachment, *Journal of Fluids and Structures* 24 (2008) 200–211.
[21] Y.L. Xu, L.Y. Wang, Analytical study of wind–rain-induced cable vibration, *Journal of Wind Engineering and Industrial Aerodynamics* 91 (2003) 27–40.
[22] D.Q. Cao, R.W. Tucker, C. Wang, A stochastic approach to cable dynamics with moving rivulets, *Journal of Sound and Vibration* 268 (2003) 291–304.
[23] N. Cosentino, O. Flamand, C. Ceccoli, Rain–wind induced vibration of inclined stay cables—part II: mechanical modeling and parameter characterization, *Wind and Structures* 6 (6) (2003) 485–498.
[24] H.P. Yuscheweyh, The mechanism of rain–wind induced vibration, in: A. Larsen, G.L. Larose, F.M. Livesey (Eds.), *Proceedings of the 10th International Conference on Wind Engineering*, Copenhagen, Denmark, Vol. 2, 21–24 June 1999, pp. 1041–1047.
[25] M. Matsumoto, et al., Motion-effect of water rivulet on rain–wind induced vibration of inclined stay-cables, *Proceedings of the Six International Symposium on Cable Dynamics*, 2005, pp. 255–262.
[26] M. Matsumoto, T. Yagi, Y. Shigemura, D. Tsusgima, Vortex-induced cable vibration of the cable-stayed bridges at high reduced wind velocity, *Journal of Wind Engineering and Industrial Aerodynamics* 89 (2001) 633–647.
[27] U. Peil, O. Dreyer, Rain–wind induced vibrations of cables in laminar and turbulent flow, *Journal of Wind and Structures* 10 (1) (2007) 83–97.
[28] S.J. Gumley, Tubing systems for pneumatic averaging of fluctuating pressures, *Journal of Wind Engineering and Industrial Aerodynamics* 12 (1983) 189–228.
[29] M. Gu, X.Q. Du, Testing study on wind pressure distributions of stayed cables with an artificial rivulet, *ACTA Aerodynamics Sinica* 23 (2005) 419–424 (in Chinese).
[30] Z.Q. Huang, E.J. Ding, *Surface infiltration and its phase transformation*, Higher Education Press, 1994 (in Chinese).
[31] U. Peil, N. Nahrath, Modeling of rain–wind induced vibrations, *Journal of Wind and Structures* 6 (1) (2003) 41–52.
[32] C. Lemaitre, P. Hemon, E. Langre, Thin water film around a cable subject to wind, *Journal of Wind Engineering and Industrial Aerodynamics* 95 (2007) 1259–1271.